Articles

Role of the Background Gas in the Morphology and Optical Properties of Laser-Microstructured Silicon

Michael A. Sheehy,[†] Luke Winston,[†] James E. Carey,[‡] Cynthia M. Friend,*,[†,‡] and Eric Mazur[‡]

Department of Chemistry, Harvard University, 12 Oxford Street, Cambridge, Massachusetts 02138, and Division of Engineering and Applied Science, Harvard University, 9 Oxford Street, Cambridge, Massachusetts 02138

Received June 17, 2004. Revised Manuscript Received May 3, 2005

We irradiated silicon with a train of femtosecond pulses in the presence of SF_6, H_2S, H_2, SiH_4, and a mixture of Ar and SF_6 in order to analyze the role of the background gas in determining the morphology and the optical properties of the resultant surfaces. We discuss factors that affect the surface morphology created during irradiation and show that the presence of sulfur in these gases is important in creating sharp microstructures. We also show that the presence of sulfur is necessary to create the near-unity absorptance for both above-band and below-band gap radiation (0.25−2.5 μm) by silicon; only samples with sulfur concentrations higher than 0.6% absorb 95% for above-band gap radiation and have a flat, featureless absorptance of 90% for below-band gap radiation.

Introduction

In the past several years, the use of lasers to incorporate impurities into silicon has produced a wealth of possibilities for new optoelectronic device applications. Of particular interest is the possibility of extending the response of silicon to wavelengths beyond the band edge, with potential applications ranging from silicon-based infrared detectors to improved solar cells.[1−3]

Her et al. first reported the formation of sharp conical microstructures by femtosecond laser irradiation of silicon in the presence of 500 Torr of SF_6.[4] The conical microstructures are on the order of 10 μm tall, have a diameter at the tip of less than 1 μm, and are quasi-periodic across the surface. The physical and chemical mechanisms for creating this microstructured surface are complex and include laser ablation and melting of the silicon substrate, substrate etching by reactive ions and fragments created in the intense fields of the laser,[5] and redeposition of material from the ablation plume.

The optical properties of the microstructured silicon are of interest because the absorptance changes over a broad range of wavelengths. For large areas of microstructured silicon, Wu et al. measured high absorptance at wavelengths from 0.25 to 2.5 μm for samples created in SF_6.[6] In the region from 0.25 to 1.1 μm, samples absorb 95% of incident radiation; at 1.1 μm, corresponding to the band gap of crystalline silicon, the absorptance decreases somewhat, but remains at 90% up to wavelengths as long as 2.5 μm.

The optical properties of microstructured silicon depend strongly on the gaseous species present during irradiation. Younkin et al. found that samples created in N_2, Cl_2, and air show enhanced optical absorptance for above-band gap radiation, but have an absorptance that decreases monotonically from the band edge (1.1 μm) to 2.5 μm.[7] To determine the source of the differences in absorptance for infrared radiation between samples created in SF_6 and samples from other background gases, the authors took Rutherford backscattering data measurements. They found 1% of sulfur in samples that had 90% absorptance for infrared radiation. Based on these Rutherford backscattering measurements and because sulfur in low concentrations is known to create discrete or localized energy states in the band gap of silicon, the authors conclude that the near-unity optical absorptance in the infrared is due to the presence of high concentrations of sulfur impurities.[8] Experimental results show that impurity concentrations on the order of 10^{16} cm^{-3} are sufficient to create an entire band of states in the gap.[9]

* To whom correspondence should be addressed. E-mail: friend@chemistry.harvard.edu.
[†] Department of Chemistry.
[‡] Division of Engineering and Applied Science.

(1) Sclar, N. *J. Appl. Phys.* **1981**, *52*, 5207.
(2) Bakhadyrkhanov, M. S.; Iliev, K. M.; Tachilin, S. A. *Appl. Sol. Energy* **1997**, *4*, 73.
(3) Wang, S. L.; Taylor, P. C. *Solid State Commun.* **1995**, *95* (6), 361.
(4) Her, T.-H.; Finlay, R. J.; Wu, C.; Deliwala, S.; Mazur, E. *Appl. Phys. Lett.* **1998**, *73* (12), 1673.
(5) Chuang, T. J. *J. Chem. Phys.* **1981**, *74*, 1453.
(6) Wu, C.; Crouch C. H.; Zhao, L.; Carey, J. E.; Younkin, R. J.; Levinson, J. A.; Mazur, E.; Farrel, R. M.; Gothoskar, P.; Karger, A. *Appl. Phys. Lett.* **2001**, *78* (13), 1850.
(7) Younkin, R.; Carey, J. E.; Mazur, E.; Levinson, J. A.; Friend, C. M. *J. Appl. Phys.* **2003**, *93*, 2626.
(8) Janzen, E.; Stedman, R.; Grossman, G.; Grimmeiss, H. G. *Phys. Rev. B* 1**984**, *29* (4), 1907.

10.1021/cm049029i CCC: $30.25 © 2005 American Chemical Society
Published on Web 06/09/2005

Younkin et al. also examined the effect of the background gas on the morphology of the resulting microstructures.[7] Microstructures formed in SF_6 and Cl_2 are sharper and twice as dense as those formed in N_2 and air. This difference is attributed to the ability of halogens to create volatile compounds of silicon, which nitrogen and oxygen do not.

Crouch et al. analyzed the crystallinity of the samples using transmission electron microscopy.[10] They found that the outer layer of the microstructures, a layer that is several hundred nanometers thick, consists of silicon nanocrystallites embedded in an amorphous and polycrystalline silicon network.

To gain a deeper understanding of the factors affecting the optical properties and morphology of these samples, we compare the morphologies and the optical properties of the structured surfaces created in H_2S, SF_6, SiH_4, H_2, and a mixture of Ar and SF_6. The work presented here provides new insight into the chemistry that leads to the formation of sharp microstructures as well as some of the critical factors for attaining near-unity absorptance over a broad range of wavelengths.

Experimental Section

For all experiments described in this paper, we used high resistivity ($\rho = 800-1200$ Ωcm), *n*-doped, Si(111) wafers cut into 10×10 mm^2 pieces. The samples were loaded into a stainless steel vacuum chamber and evacuated to about 50 mTorr using a corrosion-resistant mechanical pump. Subsequently, the system was backfilled to a pressure of 500 Torr with a specific gas or mixture. For the pure gases, we backfilled the chamber to 500 Torr via a gas-handling manifold. In experiments using a mixture of Ar and SF_6, the desired quantity of SF_6 was first added to the chamber. The manifold was then evacuated and backfilled with argon to bring the total pressure to 500 Torr with argon.

All microstructuring was done using a 1-kHz train of 100-fs, 800-nm laser pulses with a fluence of 10 kJ/m^2 focused to a spot of 150 μm in diameter. The sample was translated horizontally at 250 μm/s and stepped vertically 75 μm at the end of each row to create near uniform exposure to the laser over large areas of silicon. With the parameters listed above, approximately 600 pulses irradiate each spot on the surface.

We annealed microstructures formed in the presence of H_2S in a separate stainless steel chamber with a base pressure of 2×10^{-6} Torr in order to monitor changes in the morphologies and the optical properties of samples annealed at different temperatures. The samples were clamped to a tantalum foil and a thermocouple was spot-welded to one of these clamps, ensuring good mechanical contact between the thermocouple and the sample surface. The sample was radiatively heated to the desired temperature by a tungsten filament. The sample was annealed for 30 min at the desired temperature and the background pressure never exceeded 5×10^{-4} Torr.

To measure the optical properties of the samples, we measured the infrared absorptance with an UV−Vis spectrophotometer equipped with an integrating sphere detector. The reflectance (R) and transmittance (T) were measured for wavelengths in the range of 0.25−2.5 μm, in 1-nm increments. The absorptance ($A = 1 - R - T$) was then plotted versus the wavelength. (We use the term absorptance because it is a calculated, quantitative measure of the amount of absorption that occurs in the material; this calculated value allows quantitative comparison.)

(9) Pankove, J. I. *Optical Processes in Semiconductors*; Dover: New York, 1971.
(10) Crouch, C. H.; Carey, J. E.; Shen, M.; Mazur, E.; Genin, F. *Appl. Phys. A* **2004**, *79* (7), 1635.

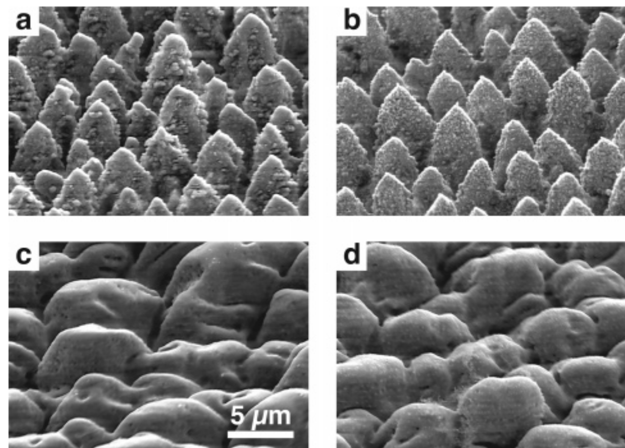

Figure 1. Scanning electron micrographs of surfaces created in the presence of (a) H_2S, (b) SF_6, (c) SiH_4, and (d) H_2.

We used Rutherford backscattering measurements to study the chemical composition of the microstructured samples. We first dipped the samples for 10 min in a 10% HF solution to remove the native oxide, then rinsed the sample, and placed it in the backscattering chamber. The backscattering measurements were taken with 2.0-MeV alpha particles and an annular solid-state detector. We determined the composition of the samples by fitting the data to simulated spectra.[11] In all simulations, the thickness of the doped layer was taken as 200 nm. This thickness was chosen based on the best fit as well as the transmission electron microscopy results in ref 10.

Results

Figure 1 shows scanning electron microscope images of surfaces prepared in H_2S, SF_6, H_2, and SiH_4. The surfaces prepared in SF_6 and H_2S have nearly identical microstructures, are approximately 10 μm tall, and are 5 μm × 3 μm wide at the base. The radius of curvature at the tip is slightly less than 1 μm and the average tip-to-tip spacing is about 4 μm. The sides of the microstructures are covered with nanometer-scale dendritically shaped material. Figure 1 also shows that the microstructures formed in the presence of H_2 and SiH_4 have a blunter shape than those formed in the presence of H_2S and SF_6 and are 10−12 μm in height and 4 μm × 10 μm wide at the base. The microstructures have a much greater area at the tip (4 μm × 8 μm) and a tip-to-tip spacing of 6 μm. The number and density of the dendritic nanoparticles are lower than those formed in the presence of H_2S and SF_6.

Samples irradiated in the presence of H_2S and SF_6 are black to the eye, while those irradiated in the presence of gases that do not contain sulfur are dull gray. Figure 2 shows the optical absorptance for the silicon samples prepared in H_2, SiH_4, SF_6, and H_2S, along with the absorptance for an unstructured silicon substrate. The microstructured surfaces' absorptance at wavelengths from 0.25 to 1.1 μm is 50% higher than crystalline silicon. Samples irradiated in the presence of H_2S and SF_6 absorb 95% for above-band gap

(11) http://www.genplot.com.

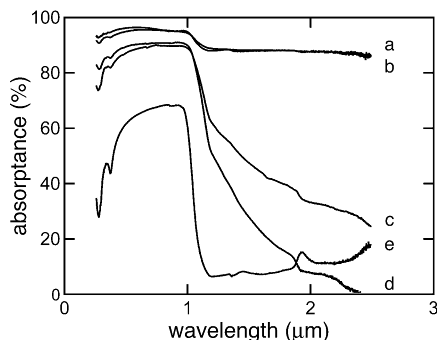

Figure 2. Infrared absorptance for surfaces created in the presence of (a) H_2S, (b) SF_6, (c) SiH_4, and (d) H_2. A trace for crystalline silicon (e) is included for reference.

Table 1. Sulfur Content and Absorptance at 2 μm of Surfaces Created in the Presence of Various Gases at a Total Pressure of 500 Torr

gas	absorptance at 2 μm	sulfur content (±0.2%)
H_2S	90%	1.0 ± 0.2%
SF_6	90%	1.0 ± 0.2%
Ar + 1% SF_6	90%	0.6 ± 0.2%
Ar + 0.1% SF_6	60%	0.2 ± 0.2%
SiH_4	33%	<0.1%[a]
Ar	15%	<0.1%[a]
H_2	8%	<0.1%[a]

[a] Because of the lack of crystallinity of the samples and because the sulfur peak is nearly enveloped by the broad silicon peak, the detection limit of our measurements is estimated to be on the order of 0.1%.

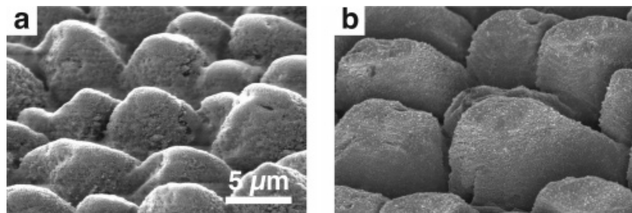

Figure 3. Scanning electron micrographs of structures created in the presence of (a) 1% partial pressure of SF_6 and (b) 0.1% partial pressure of SF_6.

radiation; those in H_2 and SiH_4 absorb 90% for above-band gap radiation.

Figure 2 also shows the below-band gap absorptance from 1.1 to 2.5 μm. Samples irradiated in the presence of H_2S and SF_6 have flat, featureless 90% absorptance for incident radiation in this wavelength range. Surfaces irradiated in the presence of H_2 and SiH_4 have an absorptance that falls monotonically for wavelengths longer than 1.1 μm. Table 1 provides a metric of the absorptance at 2 μm for each of the samples listed above that displays the changes described qualitatively above.

Figure 3 shows how the morphology of the microstructures depends on the partial pressure of the sulfur-containing gas. Microstructures formed in the presence of low partial pressures of sulfur more closely resemble microstructures created in pure H_2 and SiH_4 than those created in pure H_2S and SF_6. Individual microstructures from a 0.1% SF_6 sample (partial pressure of 500 mTorr) are 8 μm tall and 13 μm × 7 μm at the base. The structures taper to 8 μm × 3 μm at the tip and the average tip-to-tip spacing is on the order of 8 μm. Those created in 1% SF_6 (partial pressure of 5 Torr) are 9 μm tall and 8 μm × 4.5 μm at the base and taper to

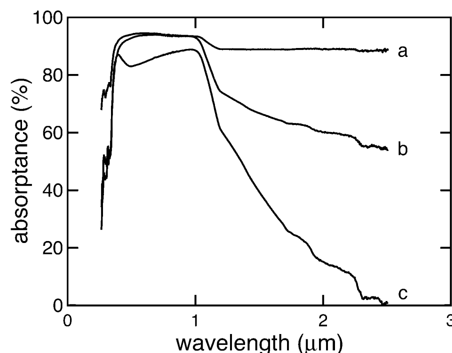

Figure 4. Infrared absorptance for surfaces created in (a) 1% SF_6, (b) 0.1% SF_6, and (c) Ar.

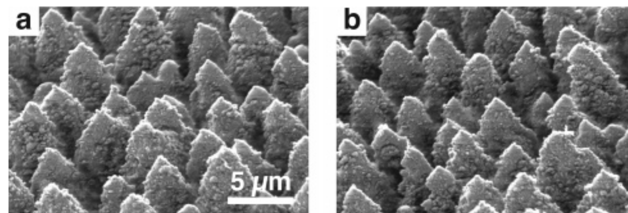

Figure 5. Scanning electron micrographs of structures created in (a) H_2S and annealed to (b) 900 K.

4 μm × 2 μm at the tip (Figure 3). The tip-to-tip spacing is approximately 6 μm for these structures, making them slightly higher in areal density than those from 0.1% SF_6. Microstructures formed in either 0.1% SF_6 or 1% SF_6 also have very little nanostructure on the sides, similar to the microstructures formed in pure H_2 and SiH_4.

Figure 4 shows the absorptance for the microstructured surfaces created in mixtures of argon and sulfur and that of a sample created in pure argon. There is an increase in both above-band and below-band gap absorptance of the samples created in low partial pressures of sulfur compared to the absorptance of samples created in H_2 and SiH_4; the absorptance of the sample created in argon decreases monotonically for wavelengths longer than 1.1 μm closely resembling that of the samples created in H_2 and SiH_4. Both samples created in sulfur mixtures absorb 95% for above-band gap radiation. The absorptance for below-band gap radiation can be seen qualitatively in Figure 4; quantitative values for the absorptance at 2 μm are provided in Table 1.

Scanning electron microscope images taken before and after annealing at 900 K (Figure 5) show that the morphology does not change within the resolution of the electron microscope. Figure 6 shows the optical properties of samples annealed at temperatures ranging from 475 to 900 K. All annealed samples have an absorptance of 95% for above-band gap radiation. The absorptance for below-band gap radiation decreases as the annealing temperature increases, but the absorptance remains flat and featureless. The sample annealed at 475 K absorbs 85% for below-band gap radiation (as compared to 90% absorptance for unannealed samples). Those annealed to 700, 800, and 900 K absorb 80%, 75%, and 70% for below-band gap radiation respectively and the results are summarized in Table 2.

Table 1 and Table 2 contain compositional information obtained from Rutherford backscattering. Structures created in H_2S have a sulfur content of approximately 1% and there

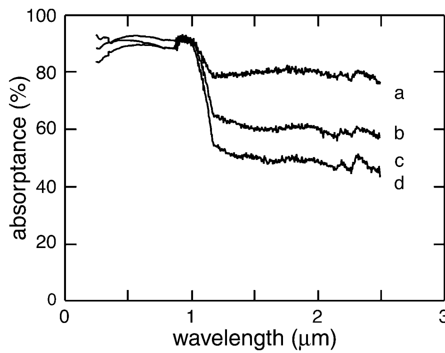

Figure 6. Infrared absorptance for H_2S surfaces annealed to (a) 475 K, (b) 700 K, (c) 800 K, and (d) 900 K.

Table 2. Dependence of the Absorptance at 2 μm and the Sulfur Content on Annealing Temperature

annealing temperature (K)	absorptance at 2 μm	sulfur content ($\pm$0.2%)
475	85%	1.0 $\pm$ 0.2%
700	80%	1.0 $\pm$ 0.2%
800	75%	1.0 $\pm$ 0.2%
900	70%	1.0 $\pm$ 0.2%

is no measurable change in the sulfur content upon annealing at 900 K. The sample created in 1% SF_6 contains 0.6% sulfur, while the 0.1% SF_6 sample has a sulfur concentration of 0.2%. We detected no sulfur in samples formed in SiH_4, H_2, or argon.

Discussion

The experimental results in Figures 1 and 3 demonstrate that the presence of sulfur in the background gas is crucial to create sharp, triangular microstructures. The fact that the morphology is nearly identical for structures created in H_2S and SF_6 indicates that the presence of H and F, common etchants of silicon with differing etch rates, are not as important as the presence of sulfur. In addition, there is a notable reduction in tip area for the individual microstructures as the amount of sulfur-containing species in the background increases. This reduction leads to a sharpening of the microstructures and an increase in the aspect ratio.

The morphology of the microstructured surfaces and the incorporation of sulfur into the surface layer are responsible for the increased absorptance at wavelengths from 0.25 to 1.1 μm. Assuming the same absorption coefficient as for crystalline silicon, two reflections on the sidewalls of the microstructured silicon increases the absorptance from approximately 70% to about 90%. These reflections can account for the increased absorptance seen in all microstructured samples, but fails to do so for the 5% increase seen in all samples created in an ambient-containing sulfur relative to that of samples created in an ambient without sulfur. The incorporation of sulfur into this outer layer must therefore create a material with an absorption coefficient that is greater than that of crystalline silicon.

Because silicon has such a small absorption coefficient in the near-infrared, multiple reflections on the sidewalls of the microstructures cannot explain the absorptance for below-band gap radiation that we observe in our samples. Damage and disorder introduced to the lattice (transmission electron microscopy results[10] indicate that the outer 200 nm of the surface is partially crystalline and partially amorphous) by femtosecond-laser irradiation and incorporation of elements of the background gas create a tail of states below the band gap by changing the bond lengths, bond angles, and/or coordination of the crystalline silicon; the extent of damage and disorder determines the width of the tail and the number of states available at each wavelength.[12] These changes to the lattice explain the below-band gap absorptance we measure in H_2, SiH_4, Ar, and 0.1% SF_6, as well as a portion of the absorptance observed in the samples created in a sulfur containing ambient.

The flat, featureless 90% absorptance for below-band gap radiation seen for samples created in H_2S, SF_6, and a mixture of 1% SF_6 and Ar, however, cannot be explained by changes in morphology nor lattice damage alone. The microstructured surfaces created in the presence of H_2S and 1% SF_6 have different morphologies, yet the infrared absorptance traces are very similar. Also, the damage done to the lattice is similar for all samples because the laser fluence is the same in all experiments. The creation of high absorptance for below-band gap radiation must therefore be the result of a parameter other than morphology or lattice damage.

Rutherford backscattering measurements indicate that the concentration of sulfur in our samples is greater than 0.6% (atomic concentration of about 10^{20} cm^{-3}) for all samples that possess a 90% absorptance for below-band gap radiation. The solid solubility of sulfur in crystalline silicon is less than 10^{15} cm^{-3} and a concentration of 0.6% of sulfur incorporated in the microstructured samples is more than sufficient to create a broad band of absorption energies. A previous study of the electronic states of sulfur in silicon identified eight discrete donor states in the gap of silicon at an atomic sulfur concentration of about 10^{16} cm^{-3}. [8] The deepest of these levels resides 614 meV below the conduction band edge.[8] If sulfur creates an entire band of states from 614 meV below the conduction band edge to the conduction band, the gap between the top of the valence band and this new band would be 456 meV, corresponding to a wavelength of 2.7 μm.

The possibility also exists that the absorptance in the near-infrared region of the spectrum is due to sulfur bonding with silicon in a highly disordered network. Excess sulfur atoms could stabilize the lattice in a nonequilibrium geometry and create a material with a greater absorption coefficient at energies below the band gap of crystalline silicon. A study on the depth distribution of ion-implanted sulfur into silicon concludes that sulfur clusters around defect sites induced by the ion beam, especially in the defect-rich transition layer between the implantation-damaged layer and the unperturbed crystalline silicon layer.[13] Given the similarity in atomic concentrations of sulfur as well as the thickness of the disordered layer between the ion-implanted samples and our microstructured samples, we expect that sulfur coordinates around any area with a high density of defects and stabilizes the network. This distribution of atoms has a new electronic configuration that may cause a broad band of absorption energies in the near-infrared.

(12) Zanatta, A. R.; Chambouleyron, I. *Phys. Rev. B* **1996**, *53* (7), 3833.
(13) Wilson, R. G. *J. Appl. Phys.* **1984**, *55* (10), 3490.

The absorptance measurements shown in Figure 6 combined with the data from Table 1 provide further evidence that the near-unity absorptance for below-band gap radiation is caused by a combination of the incorporation of sulfur and a disordered silicon network. Upon annealing to 900 K, the absorptance for below-band gap radiation drops to 70%, but the concentration of sulfur is unchanged. There are several potential explanations for the observed drop in absorptance for below-band gap radiation. One possibility is that sulfur diffuses out of an active site, which is a location in the network where sulfur is coordinated in such a way as to create below-band absorption. The diffusion coefficient for sulfur is relatively low and the annealing time is short, indicating that diffusion out of an active site is unlikely.[14] Another possibility is precipitation of the sulfur atoms into an inactive cluster. Such precipitation has been observed for arsenic implanted in silicon.[15] Precipitation of sulfur into inactive clusters requires diffusion of silicon out of an area with a high concentration of sulfur or diffusion of sulfur into this type of area. While we cannot rule out the possibility that sulfur forms precipitates, the likelihood of diffusion of either silicon or sulfur on this time scale and these temperatures is unlikely. A third possibility is a relaxation of the sulfur−silicon network that makes the electronic structure partially revert to that of crystalline silicon. Various experimental data show that thermally induced relaxations (e.g., healing of defect sites not coordinated with silicon) in amorphous silicon occur over a wide range of temperatures and depend on the distribution of bond lengths and bond angles in the amorphous network and the dopant concentrations.[16−18] In particular, changes in ion-implanted silicon occur at temperatures as low as 400 K, which is well below any of the annealing temperatures we used.[18] Because there is no change in sulfur concentration after annealing and the annealing temperatures are relatively low, thermal relaxation is likely to be the dominant mechanism for the reduction in near-infrared absorptance after annealing.

In conclusion, we show that incorporation of sulfur (on the order of 1%) into a disordered silicon network created by femtosecond laser irradiation leads to near-unity absorptance for both above- and below-band gap radiation. The presence of sulfur is also an important factor in developing sharp microstructures. The absorption mechanism for below-band gap radiation is either due to the creation of an impurity band resulting from the high concentration of sulfur or due to the incorporation of sulfur into the disordered network in such a way as to create a material with a new electronic structure. The decrease in absorptance for below-band gap radiation observed upon annealing appears to be primarily due to thermal relaxation of the disordered silicon network.

Acknowledgment. The authors thank Mengyan Shen for helpful discussions and Catherine Crouch and John Chervinsky for help with the Rutherford backscattering experiments and subsequent data fitting. Michael Sheehy acknowledges support from the NSF GK-12 program. This work was supported by MRSEC and the Department of Energy.

CM049029I

(14) Rollert, F.; Stolwijk, N. A.; Mehrer, H. *Appl. Phys. Lett.* **1993**, *63* (4), 506.
(15) La Via, F.; Privitera, V.; Lombardo, S.; Spinella, C.; Raineri, V.; Rimini, E.; Baeri, P.; Ferla, G. *J. Appl. Phys.* **1991**, *69* (2), 726.
(16) Volkert, C. A. *J. Appl. Phys.* **1993**, *74* (12), 7107.
(17) Cheng, J.-Y.; Gibson, J. M.; Baldo, P. M.; Kestel, B. J. *J. Vac. Sci. Technol. A* **2002**, *20* (6), 1855.
(18) Donovan, E. P.; Spaepen, F.; Poate, J. M.; Jacobson, D. C. *Appl. Phys. Lett*. **1989**, *55* (15), 1516.